Surface Passivation of GaAs Nanowire Ensembles for Photovoltaic Applications

A.C.E Chia , R.R. LaPierre

Department of Engineering Physics, Centre for Emerging Device Technologies,

McMaster University, Hamilton, ON, Canada, L8S 4L7

Email: lapierr@mcmaster.ca

ABSTRACT

Fabrication, electrical characterization and analytical modeling of an AlInP-passivated GaAs NW ensemble is presented. Novel processing steps were used to fabricate NW ensemble devices which were subsequently characterized electrically and fit with an analytical model, showing a 48% reduction in interface state density and an impressive four order of magnitude increase in effective carrier concentration of the NWs, rivaling the performance of other passivation schemes reported in the literature. This is the first known report of surface passivation of a NW ensemble device with a III-V shell and demonstrated by electrical characterization of a whole ensemble of NWs.

Keywords: nanowire, passivation, GaAs, VLS

1 INTRODUCTION

In recent years, there has been considerable research in the use of III-V nanowires (NWs) for optoelectronic applications by taking advantage of quantum confinement and lattice-mismatched growth allowed by the small NW diameters [1]. However, these small diameters amplify detrimental surface effects such as surface depletion and surface recombination, which have been shown to reduce optoelectronic device performance[2]. To rectify this issue, GaAs NW ensembles were surface-passivated with AlInP to form a Type I heterojunction, thus reducing surface recombination and depletion. GaAs NW ensemble devices were subsequently fabricated using novel methods and finally characterized by current-voltage (I-V) measurements. Effectiveness of passivation was assessed by comparison to I-V characteristics of a reference unpassivated GaAs NW ensemble. Finally, an analytical surface depletion model and transport model were combined to fit the I-V curves. Close-fits of the I-V characteristics showed vast improvement of carrier concentration upon passivation.

2 EXPERIMENTAL DETAILS

Core-shell GaAs-AlInP heterostructure NWs were grown by MBE using the vapour-liquid-solid (VLS) mechanism for growth. Before growth, the n-type GaAs (111)B substrate was cleaned by a series of UV ozone, buffered HF etching and rinsing steps. Following this, a 1 nm layer of Au was deposited to provide the seed particles for VLS growth. The substrates were then transferred to the MBE where a series of degassing and plasma cleaning steps were performed. The NWs were then grown, beginning with the Te-doped GaAs core segment to achieve a nominal ionized donor density of $1x10^{18}$ cm^{-3} (as calibrated by previous thin film growths), followed by the growth of an intrinsic, nominally lattice-matched $Al_{0.52}In_{0.48}P$ shell. Using the same conditions, an unpassivated reference sample was also grown excluding the AlInP shell growth. The full details of the growth conditions have been reported earlier [3].

After growth, the NW ensembles were characterized by secondary electron microscopy (SEM), while individual NWs were characterized by transmission electron microscopy (TEM) and energy dispersive x-ray spectroscopy (EDX). Subsequently, a series of processing steps were used to fabricate an ensemble NW resistor device. First, the NW ensemble was spin-coated in a 3:1 volume mixure of Cyclotene 3022-35 to T1100 thinner to fill the space between the NWs. Cyclotene was ideal for this purpose due to its low porosity, high electrical resistivity, high thermal stability and low surface roughness as previously reported [4]. Second, the sample underwent RIE in a 1:1 mixture (by flow rate) of O_2 and CF_4 in order to back-etch the Cyclotene layer to a height of ~1 µm. Third, the samples were sonicated in DI water for 60 minutes. This caused the tops of the NWs protruding from the polymer to break off to achieve complete planarization. Additionally, since the tops of the NWs consisted of the highly resistive AlInP segment covering the GaAs cores, this step served to expose the GaAs cores for electrical contacting. Finally, electron beam evaporation was used to deposit an array of 0.5 mm^2 top contact pads composed of 50 nm Ni, 100 nm Ge and 650 nm Au, and a bottom substrate contact composed of 25 nm Ni, 50 nm Ge and 120 nm Au.

Once fabricated, effectiveness of passivation was examined by using a two-point probe system to compare I-V characteristics between both passivated and unpassivated

NW devices when probed at the top and bottom contacts (shown schematically in Figure 1a). In this work, positive bias corresponds to the situation whereby the top of the NWs are held at a potential, $+V$, while the bottom of the substrate is tied to ground.

3 RESULTS

SEM of the samples found that a dense NW ensemble was grown (NW density ≈ $2\text{x}10^9$ cm^{-2}) with heights ranging from 1 to 2.5 µm. The radius of the GaAs cores varied from 10 to 36 nm, while the thickness of the AlInP shell was found to vary from 5 to 45 nm according to high angle annular dark field (HAADF) TEM. Using EDX, the $Al_xIn_{1-x}P$ shells were confirmed to be lattice matched to GaAs, having a mean composition of x=0.52 with a standard deviation of 0.03. Electron microscopy analysis on these samples has been previously reported in detail [3].

Processing steps were also found by SEM to successfully fabricate the structure shown in Figure 1a. I-V measurements described below indicated that the AlInP shells conducted negligible current, hence necessitating the underlying n-doped GaAs cores to be contacted instead of the undoped AlInP shells to achieve low contact resistance. Sonication was found to be particularly successful in removing the axial AlInP segments atop of the GaAs cores as shown in Figure 2. From this figure, the core-shell structure is readily apparent whereby the GaAs cores are exposed for ohmic front contact formation.

Figure 1b shows I-V characteristics of passivated and unpassivated NW devices which are colour-coded to correspond with the various probe configurations shown in Figure 1a. If must first be noted that a parasitic 3Ω series resistance exists in the measurement apparatus which is represented in the subsequent model by parameter R_s. I-V curves measured across Contact A (green triangles) and across the GaAs film at Contact C (blue triangles) had resistances equal to the parasitic series resistance, demonstrating that the contacts and film have negligible contributions to the overall series resistance. Secondly, it is readily observed that the I-V curves show a two order of magnitude current increase with passivation (red triangles) versus without passivation (black triangles). To show that this current increase did not occur due to conduction through the AlInP shell, further I-V measurements of passivated NWs (not shown) with the axial AlInP sections left intact were found to draw two orders of magnitude less current than the unpassivated NWs. As such, the increase in current qualitatively suggests successful passivation.

4 MODEL

To quantify the extent of surface depletion and passivation, the I-V characteristics were fit using an integration of two models: a surface depletion model and a transport model. The depletion model was taken entirely from previously published work by Chia and LaPierre [5]

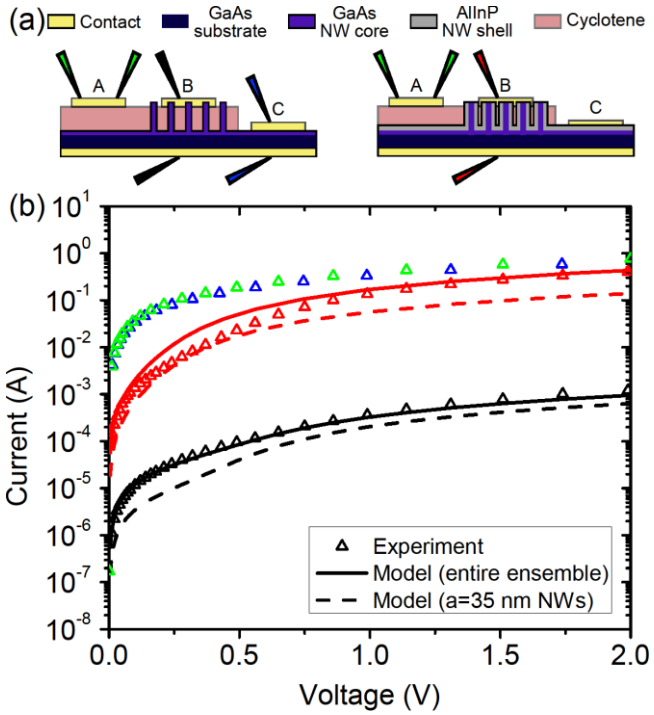

Figure 1: (a) Schematic of the three different top contacts deposited on unpassivated (left) and passivated (right) NW devices with varying two-point probe configurations. (b) I-V measurements across a single contact pad (green), the GaAs substrate alone (blue), passivated NWs (red) and unpassivated NWs (black). Model-generated I-V curves (solid lines) of the entire ensemble and that from the upper 1% of NW diameters (dashed lines). The colours of the curves correspond with the probe colours in (a).

and gives the Fermi level position along with the conduction and valence band profiles as a function of radial position. This allows for the calculation of effective carrier concentrations needed for the subsequent transport model, which models the NW ensemble as an equivalent circuit and generates fits to the I-V curves.

4.1 Surface depletion model

Key findings from Chia and LaPierre [5] relevant to the subsequent transport model are summarized below. Poisson's equation was solved in cylindrical coordinates to give the potential as a function of radius, $\psi(r)$, defined as the potential difference between the radially changing intrinsic level, E_i, and the constant Fermi level, E_f where the potential is zet at zero.

For a NW that is partially depleted, the potential is given by

$$\psi(r)=\begin{cases}\psi_0 & \text{for } 0<r<r_q \\ \psi_0+\dfrac{qN_Dr_q^2}{2\varepsilon}\left[-\dfrac{r^2}{2r_q^2}+\ln\left(\dfrac{r}{r_q}\right)+\dfrac{1}{2}\right] & \text{for } r_q<r<a\end{cases} \quad (1)$$

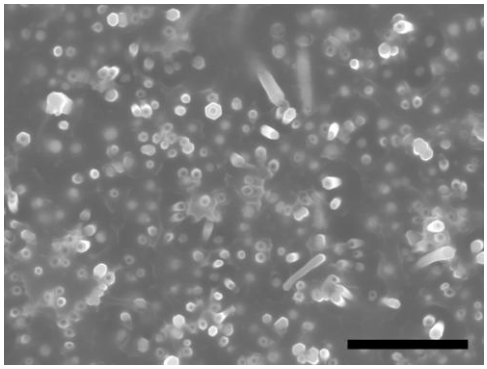

Figure 2: Top view SEM of sonicated NWs displaying both the GaAs cores and AlInP passivation shells. The scale bar is 1µm.

where ε is the permittivity of GaAs, q is the elementary charge, N_D is the donor doping density, r_q is the radius of the quasi-neutral core region of the NW, ψ_0 is the potential along the centre axis of the NW and a is the radius of the GaAs core. While N_D and a are generally known, ψ_0 and r_q must be determined for $\psi(r)$ to be explicitly expressed. A transcendental equation in ψ_0 can be found and solved:

$$\frac{2}{\sqrt{\pi}} N_c F_{1/2}(\eta_{F0}) = N_D^+ \quad \text{where} \quad \eta_{F0} = \frac{q\psi_0 - E_g/2}{kT} \tag{2}$$

where $F_{1/2}(\eta)$ is the Fermi-Dirac integral, N_c is the effective density of states in the conduction band, E_g is the energy bandgap, k is the Boltzmann constant, and T is the temperature. r_q is found by solving the transcendental equation:

$$\frac{\left(a^2 - r_q^2\right) qN_D}{2aq^2 D_{it}} - \frac{E_g}{2q} + \psi_{\text{CNL}} = \frac{qN_D r_q^2}{2\varepsilon}\left[-\frac{a^2}{2r_q^2} + \ln\left(\frac{a}{r_q}\right) + \frac{1}{2}\right] + \psi_0 \tag{3}$$

where D_{it} is the density of interface states at the GaAs surface and ψ_{CNL}=0.53V is the charge neutrality level (CNL) for GaAs [6].

For a NW that is fully depleted (r_q = 0), the potential is given by

$$\psi(r) = \psi_0 - \frac{qN_D}{4\varepsilon} r^2 \quad \text{for} \quad 0 < r < a \tag{4}$$

In this case, ψ_0 cannot be calculated in the same way as the partially depleted regime, but is given by

$$\psi_0 = \frac{aN_D}{2qD_{it}} - \frac{E_g}{2q} + \psi_{\text{CNL}} + \frac{qN_D}{4\varepsilon} a^2 \tag{5}$$

From Eqn (1) to (5), $\psi(r)$ can be explicitly expressed for all combinations of D_{it}, a and N_D values.

4.2 Transport model

To relate the surface depletion model-generated $\psi(r)$ to carrier transport, one must first determine the free electron and hole concentrations, $n(r)$ and $p(r)$ respectively, using the Fermi-Dirac integral. Then, for a particular nanowire, NW_i, the effective free carrier densities can be written as

$$n_{\text{eff,i}} = \frac{1}{\pi a_i^2} \int_0^{a_i} n(r) 2\pi r dr \tag{6}$$

$$p_{\text{eff,i}} = \frac{1}{\pi a_i^2} \int_0^{a_i} p(r) 2\pi r dr \tag{7}$$

With the effective carrier concentrations, all necessary transport equations can be solved. The NW ensemble device was modeled with an equivalent circuit shown in Figure 3. Each parallel branch in Figure 3 represents a single NW and is composed of a diode D_i, series resistor R_i and identical leakage resistor R_{lk}.

The diode, D_i, arises because surface depletion of the NW causes an n^+n junction to be formed at the substrate-NW interface. The reverse saturation current through D_i can be expressed as

$$I_{0,i} = \pi a_i^2 q\left(\frac{D_p p_{sub}}{L_p} + \frac{D_n n_{\text{eff},i}}{L_n}\right) \tag{8}$$

where D_n, L_n and $n_{eff,i}$ are the diffusion coefficient, diffusion length and effective carrier concentration for electrons in NW_i, while D_p, L_p and p_{sub} are the diffusion coefficient, diffusion length and carrier concentration for holes in the n-doped substrate.

The resistor, R_i, represents the resistance of NW_i itself as given by the surface depletion model

$$R_i = \frac{1}{q(\mu_e n_{\text{eff},i} + \mu_p p_{\text{eff},i})} \frac{L}{\pi a_i^2} \tag{9}$$

where μ_e is the electron mobility, μ_p is the hole mobility and L is the length of the NW.

The resistor, R_{lk}, represents possible leakage paths through which current can bypass the NWs. Current leakage has been observed previously[7].

Standard circuit analysis then gives that the current flowing through a single NW is given by

$$I_i(V') = I_{0,i}\left[\exp\left(\frac{q(V' - I_i R_i)}{nkT}\right) - 1\right] + \frac{V' - I_i R_i}{R_{lk}} \tag{10}$$

where n is the ideality factor and V' is the voltage drop across each branch in Figure 3 such that the applied bias is given by $V = V' + IR_s$. To fit the experimental I-V data, I_i is summed for all NWs of varying radius under the contact pad to yield the total current, I.

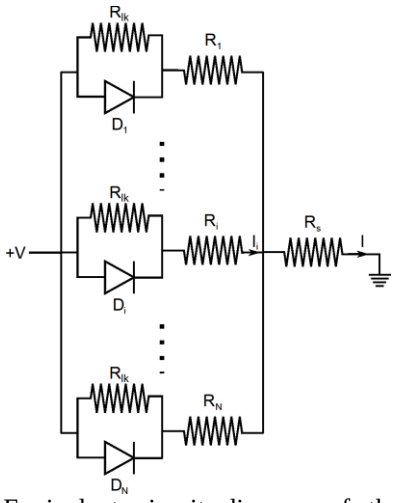

Figure 3: Equivalent circuit diagram of the ensemble device.

5 ANALYSIS AND DISCUSSION

Using the reasonable fit parameters given in Table 1, a close fit to the I-V curves in Figure 1b was found for D_{it}=5.8x10^{12} cm^{-2}eV^{-1} (black solid line) in unpassivated NWs and D_{it}=3.0x10^{12} cm^{-2}eV^{-1} (red solid line) in passivated NWs, marking an excellent 48% improvement. Figure 1b also shows a current similar in magnitude drawn by merely the a~35 nm NWs (dashed lines), which represent the highest 1% of the NW ensemble radius distribution. This shows that these a~35 nm NWs dominate the device performance due to their low relative resistance. Examining these characteristic a~35 nm NWs further, the best-fit D_{it} values correspond to n_{eff}=6.1x10^{13} cm^{-3} for unpassivated NWs and n_{eff}=1.7x10^{17} cm^{-3} for passivated NWs, marking a four order of magnitude improvement.

6 CONCLUSIONS

In conclusion, fabrication and passivation of an ensemble NW device has been demonstrated. Novel fabrication steps were used to remove top axial AlInP segments for subsequent contacting. I-V characteristics of passivated and unpassivated NWs were measured and fit with a surface depletion and transport model, yielding an excellent 48% reduction of surface state density upon passivation. Furthermore, the thickest NWs in the ensemble were found to dictate the device characteristics despite amounting to only 1% of the entire ensemble. This serves as an example of how the surface depletion and transport models provide excellent tools to give insight into the effect of surface depletion in a variety of different semiconductor NWs

Table 1: Key parameters used to fit I-V curves

Variable	Value	Reference/Source
N_D	1x10^{18} cm^{-3}	known
L	900 nm	SEM
μ_e	3000 cm^2 V^{-1} s^{-1}	[6]
μ_p	150 cm^2 V^{-1} s^{-1}	[6]
τ_p	1 ns	[8]
τ_n	1 µs	[8]
R_{lk}	1.2 GΩ	[7]
n	3	[9]

REFERENCES

[1] H. J. Joyce, Q. Gao, H. Hoe Tan, C. Jagadish, Y. Kim, J. Zou, L. M. Smith, H. E. Jackson, J. M. Yarrison-Rice, P. Parkinson, and M. B. Johnston, "IIIâ€"V semiconductor nanowires for optoelectronic device applications," *Progress in Quantum Electronics*, vol. 35, pp. 23–75, Mar. 2011.

[2] L. J. Lauhon, M. S. Gudiksen, and C. M. Lieber, "Semiconductor nanowire heterostructures.," *Philosophical transactions. Series A, Mathematical, physical, and engineering sciences*, vol. 362, pp. 1247–60, June 2004.

[3] A. C. E. Chia, M. Tirado, Y. Li, S. Zhao, Z. Mi, D. Comedi, and R. R. LaPierre, "Electrical transport and optical model of GaAs-AlInP core-shell nanowires," *Journal of Applied Physics*, vol. 111, no. 9, p. 094319, 2012.

[4] A. C. E. Chia and R. R. LaPierre, "Contact planarization of ensemble nanowires.," *Nanotechnology*, vol. 22, p. 245304, June 2011.

[5] A. C. E. Chia and R. R. LaPierre, "Analytical model of surface depletion in GaAs nanowires," *Journal of Applied Physics*, vol. 112, no. 6, p. 063705, 2012.

[6] S. Sze and K. K. Ng, *Physics of Semiconductor Devices*. Hoboken, NJ, USA: John Wiley & Sons, Inc., Oct. 2006.

[7] O. Salehzadeh, M. X. Chen, K. L. Kavanagh, and S. P. Watkins, "Rectifying characteristics of Te-doped GaAs nanowires," *Applied Physics Letters*, vol. 99, no. 18, p. 182102, 2011.

[8] M. Levinshtein and M. Shur, *Handbook Series on Semiconductor Parameters*. World Scientific Publishing Company, Incorporated, v. 2 ed., 1995.

[9] F. Léonard, A. Talin, B. Swartzentruber, and S. Picraux, "Diameter-Dependent Electronic Transport Properties of Au-Catalyst/Ge-Nanowire Schottky Diodes," *Physical Review Letters*, vol. 102, pp. 1–4, Mar. 2009.